Tension and Stiffness of the Hard Sphere Crystal-Fluid Interface

A. Härtel,[1] M. Oettel,[2] R. E. Rozas,[1] S. U. Egelhaaf,[3] J. Horbach,[1] and H. Löwen[1]

[1]*Institut für Theoretische Physik II: Weiche Materie, Heinrich-Heine-Universität Düsseldorf, Universitätsstraße 1, D-40225 Düsseldorf, Germany*

[2]*Johannes-Gutenberg-Universität Mainz, Institut für Physik, WA 331, D-55099 Mainz, Germany*

[3]*Condensed Matter Physics Laboratory, Heinrich-Heine-Universität Düsseldorf, Universitätsstraße 1, D-40225 Düsseldorf, Germany*

(Received 13 March 2012; published 29 May 2012)

A combination of fundamental measure density functional theory and Monte Carlo computer simulation is used to determine the orientation-resolved interfacial tension and stiffness for the equilibrium hard-sphere crystal-fluid interface. Microscopic density functional theory is in quantitative agreement with simulations and predicts a tension of $0.66 k_B T/\sigma^2$ with a small anisotropy of about $0.025 k_B T$ and stiffnesses with, e.g., $0.53 k_B T/\sigma^2$ for the (001) orientation and $1.03 k_B T/\sigma^2$ for the (111) orientation. Here $k_B T$ is denoting the thermal energy and σ the hard-sphere diameter. We compare our results with existing experimental findings.

DOI: 10.1103/PhysRevLett.108.226101 PACS numbers: 68.08.De, 05.20.Jj, 64.70.D−, 82.70.Dd

Solidification and melting processes involve crystal-fluid interfaces that separate the disordered from the ordered phase. Understanding the properties of such interfaces on a microscopic scale is pivotal to control and optimize crystal nucleation and the emerging microstructure of the material. Important applications include the fabrication of defect-free metallic alloys [1] and of photonic [2], phononic [3], and protein [4] crystals. In equilibrium, i.e., between a coexisting crystal and fluid phase, creating a crystal-fluid interface results in a free energy penalty per area that is called interfacial tension. Unlike the liquid-gas or fluid-fluid interface, the structure of the solid-fluid interface depends on its orientation [5]. This anisotropy is associated with a difference between the interfacial tension and the interfacial stiffness of a crystalline surface.

Predicting crystal-fluid interfacial tensions by a molecular theory is a very challenging task. Classical density functional theory of freezing provides a unifying framework to describe the solid and liquid on the same footing and is therefore in principle a promising tool. In this respect, the simple athermal hard-sphere system which exhibits a freezing transition from a fluid into a face-centered-cubic (fcc) crystal, is an important reference system. The accuracy of previous density functional calculations of the hard-sphere solid-fluid interface [6–9], however, was hampered by the lack of knowledge of a reliable functional and severe restrictions in the parametrization of the trial density profile.

In this Letter, interfacial tensions and stiffnesses of the equilibrium hard-sphere crystal-fluid interface are predicted using fundamental measure density functional theory [10] which has been shown to predict accurate bulk freezing data [11]. The interfacial tension and stiffness for five different orientations are obtained, namely, along the (001), (011), (111), (012), and (112) orientations (see Fig. 1). A small orientational anisotropy for the tensions is found and the average tension is about $0.66 k_B T/\sigma^2$ with $k_B T$ denoting the thermal energy and σ the hard-sphere diameter. For the stiffnesses the data are spread in a much wider range between $0.28 k_B T/\sigma^2$ for the (011) orientation with lateral direction $[\bar{1}00]$ and $1.03 k_B T/\sigma^2$ for the (111) orientation. We have also conducted Monte Carlo simulations to extract the stiffness from capillary-wave fluctuations for the above orientations except (012), thereby improving the accuracy of earlier data [12–18]. We find quantitative agreement between density functional theory and computer simulation.

In equilibrium, the athermal hard-sphere model system is solely characterized by the volume fraction ϕ; the thermal energy $k_B T$ just sets the energy scale. The fluid-solid (fcc) freezing transition is first-order with coexisting fluid and solid volume fractions of $\phi_f = 0.492$ and $\phi_s = 0.545$, respectively, and a coexistence pressure of $p_c = 11.576 k_B T/\sigma^3$ [19]. For a given volume V containing coexisting bulk fluid and solid, and a planar fluid-solid interface of area A, the excess grand free energy per area

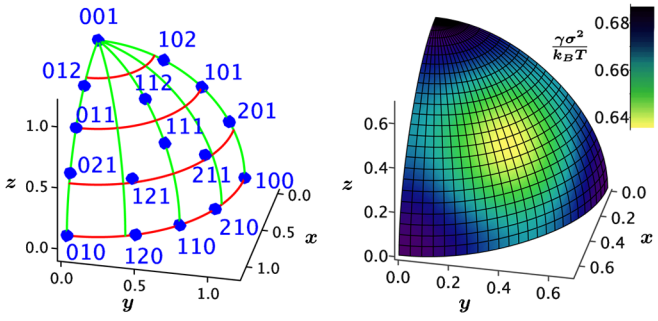

FIG. 1 (color online). In the left panel, the surface orientations, as listed in Table I, are indicated on an octant of the unit sphere. The right panel shows a Wulff plot of the corresponding interfacial tension $\gamma(\hat{n})$; here, the colors display the value of the tension for a given orientation.

is the surface or interface tension, given by $\gamma = (\Omega + pV)/A$, with Ω denoting the grand-canonical free energy. For crystal-fluid interfaces, γ depends on the orientation of the interface, characterized by a normal unit vector $\hat{n}$ relative to the crystal lattice. The latter is fixed with the fcc cubic unit cell edges parallel to the Cartesian coordinate axes of our system, see Fig. 1.

The central quantity to describe thermal fluctuations, i.e., capillary waves, along the anisotropic crystal-fluid interface is the interfacial stiffness defined tensorially [20] as

$$\bar{\gamma}_{\alpha\beta}(\hat{n}) = \gamma(\hat{n}) + \frac{\partial^2 \gamma(\hat{n})}{\partial \hat{n}_\alpha \partial \hat{n}_\beta} \tag{1}$$

for two directions $\hat{n}_\alpha$ and $\hat{n}_\beta$ that are orthogonal to $\hat{n}$.

We calculate the tension of the hard-sphere crystal-fluid interface using classical density functional theory (DFT) that provides direct access to the grand-canonical free energy Ω [21]. We employ the geometric fundamental measure approach first established by Rosenfeld [22,23] and most accurately refined in the so-called White Bear version mark II [10]. A free minimization of this theory in the bulk phases [11] gives accurate hard-sphere bulk coexistence data which are needed as a reliable input for the calculation of interfacial tensions. The crystal-fluid phase transition occurs at a coexistence chemical potential $\mu_c/k_BT = 16.3787$ and a coexistence pressure $p_c\sigma^3/k_BT = 11.8676$. The coexistence packing fractions of the fluid and solid are, respectively, $\phi_f = 0.495$ and $\phi_s = 0.544$, in close agreement with the aforementioned computer simulation data [19].

At the prescribed coexistence chemical potential μ_c, the grand free energy functional is numerically minimized inside a rectangular cuboid box of lengths L_x, L_y, and L_z with periodic boundary conditions in all three directions [7]. The surface normal is pointing along the z direction and the box length L_z is chosen large enough (about 50–60σ) to ensure a large part of bulk crystal and fluid phase at coexistence which are separated by two interfaces. The lateral dimensions L_x and L_y of the box depend on the surface orientation relative to the fcc crystal. They are determined by the minimal size of a periodic rectangular cross section which accommodates the prescribed relative orientation. The density field is resolved on a fine rectangular grid in real space with a spacing of about 0.02σ. Starting from an initial profile which contains the two bulk parts of preminimized crystal and fluid, the density functional is minimized using a Picard iteration scheme combined with a direct inversion in the iterative subspace method [24,25] and a simulated annealing technique [7]. Finite size effects due to the finite grid size were excluded by also using smaller grid spacings to ensure free minimization of the density functional in practice.

Results for the minimized density profiles are displayed in Fig. 2 for five different orientations. Both the laterally integrated (z-resolved) density field $\bar{\rho}(z) = \frac{1}{L_xL_y} \times \int_0^{L_x}\int_0^{L_y} \rho(x, y, z)dydx$ and contour plots, $\rho(x = 0, y, z)$, are shown.

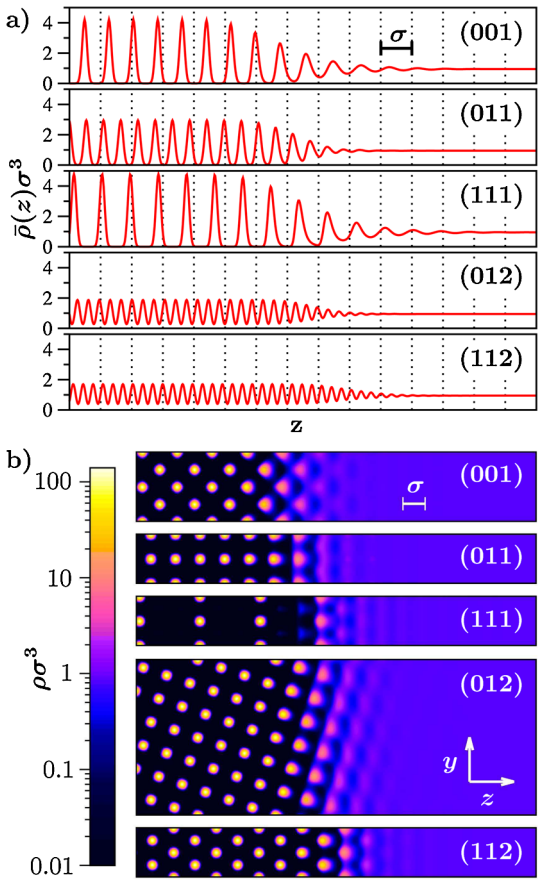

FIG. 2 (color online). DFT results: (a) Laterally integrated density profiles $\bar{\rho}(z)$ for the five surface orientations, as indicated, (b) contour plots at $x = 0$. The periodic length of the total profiles in z direction is 50.15σ (001), 53.19σ (011), 65.15σ (111), 56.07σ (012), and 61.42σ (112).

The DFT results for the interfacial tension are summarized in Table I for five different orientations. With a slight orientational dependence, all the values vary around $0.66k_BT/\sigma^2$. The errors given in Table I are estimated from several independent minimization runs. Since the anisotropy is weak, the orientational resolved interfacial tension can be well-fitted by the cubic harmonic expansion [26,27]

$$\frac{\gamma(\hat{n})}{\gamma_0} = 1 + \epsilon_1\left(Q - \frac{3}{5}\right) + \epsilon_2\left(3Q + 66S - \frac{17}{7}\right) + \epsilon_3\left(5Q^2 - 16S - \frac{94}{13}Q + \frac{33}{13}\right) \tag{2}$$

with $\hat{n} = (n_1, n_2, n_3)$, $Q = n_1^4 + n_2^4 + n_3^4$, $S = n_1^2n_2^2n_3^2$ and four fit parameters γ_0, ϵ_1, ϵ_2, ϵ_3. The expansion (2) can be used to obtain the interfacial stiffness (1) from the DFT data of the anisotropic interfacial tension [19,27]. The

TABLE I. Interfacial tensions γ and stiffnesses $\bar{\gamma}$ in units of $k_B T/\sigma^2$ for different surface normal vectors (round brackets) and tangential directions (square brackets). In DFT the tensions are measured directly, in the simulation the stiffnesses. The other data are listed italicized and are calculated using the fit function (2). The fit parameters are obtained from a least-square fit to the measured data. For DFT they are $\gamma_0 = 0.664(2) k_B T/\sigma^2$, $\epsilon_1 = 0.1076(120)$, $\epsilon_2 = -0.01364(292)$, $\epsilon_3 = -0.0023(209)$ and for simulation $\gamma_0 = 0.618(11) k_B T/\sigma^2$, $\epsilon_1 = 0.0905(32)$, $\epsilon_2 = -0.00547(44)$, $\epsilon_3 = 0.0054(25)$. As a reference previous simulation results for tensions [17] and stiffnesses [15] are shown in the last column. The numbers in parentheses indicate the uncertainty in the last digit(s).

	Orientation	Theory	Simulation	References [15,17]
γ	(001)	0.687(1)	*0.639(11)*	0.5820(19)
$\bar{\gamma}$	(001)	*0.53(14)*	0.419(5)	0.44(3)
γ	(011)	0.665(1)	*0.616(11)*	0.5590(20)
$\bar{\gamma}$	(011)[$\bar{1}$00]	*0.283(35)*	0.401(5)	0.42(3)
$\bar{\gamma}$	(011)[01$\bar{1}$]	*0.86(14)*	0.769(5)	0.70(3)
γ	(111)	0.636(1)	*0.600(11)*	0.5416(31)
$\bar{\gamma}$	(111)	*1.025(79)*	0.810(5)	0.67(4)[a]
γ	(012)	0.674(5)	*0.623(11)*	0.5669(20)
$\bar{\gamma}$	(012)[$\bar{1}$00]	*0.454(57)*	0.575(5)	0.59(3)
$\bar{\gamma}$	(012)[02$\bar{1}$]	*0.71(12)*	0.420(5)	0.43(3)
γ	(112)	0.654(1)	*0.611(11)*	
$\bar{\gamma}$	(112)[$\bar{1}$10]	*0.973(41)*	0.606(5)	
$\bar{\gamma}$	(112)[11$\bar{1}$]	*0.704(50)*	0.550(5)	

[a]This value is for the rhcp-crystal-liquid, rather than the fcc-crystal-liquid interface. See [15] for details.

resulting anisotropy of the stiffness is considerably larger than the one of the tension [thus, the resulting errors of $\bar{\gamma}_{\alpha\beta}(\hat{n})$ are also larger]. For the five different orientations considered in this work, the resulting data for the interfacial stiffness and for the fit parameters are listed in Table I.

In the Monte Carlo (MC) simulations, similar to the procedure in [12,19], inhomogeneous hard-sphere systems at the coexistence pressure p_c are prepared followed by production runs in the canonical ensemble. The canonical MC simulation consists of particle displacement moves according to a standard Metropolis criterion where the trial displacements of the particles are randomly chosen from the interval $[-0.11\sigma, +0.11\sigma]$. The inhomogeneous solid-fluid systems are placed in rectangular cuboid simulation boxes of nominal size $L \times L \times 5L$ ($L \approx 25\sigma$), containing about 10^5 particles. We apply periodic boundary conditions in all three dimensions, the fcc crystal with z extension of about $2L$ resides in the middle of the box and is separated from the fluid by two planar interfaces. Since the system is in equilibrium, the amount of crystal and fluid phase as well as the interfaces remain stable during the simulation. We consider the crystal orientations (001), (011), (111), and (112), see Fig. 1. At each orientation, 10 independent runs are performed and in each of these runs, 10 000 independent configurations are generated that are used for the analysis of the interfaces.

The stiffnesses $\bar{\gamma}$ are extracted from the capillary-wave spectrum $\langle h^2(\vec{q})\rangle$ [27], i.e., the correlation function of the interface height fluctuation $h(\vec{q})$ (with $\vec{q} = (q_x, q_y)$ the two-dimensional wave vector along the lateral extension of the interface). In order to determine $h(\vec{q})$ a criterion has to be introduced according to which one can distinguish between fluid and crystal particles. Following work [12,19], the rotational-invariant bond-order parameter $q_6 q_6(i)$ was used [28,29]. To distinguish between crystalline and fluid particles, we adopt the same criterion as in Refs. [12,19], where a particle i was identified as one with crystalline order if $q_6 q_6(i) > 0.68$, otherwise it was defined as a liquidlike particle. Moreover, the local position of the interface is defined by the set of crystalline particles at the interface (particles which have less than 11 crystalline neighbors). Some particles in the liquid bulk identified as crystalline were removed by searching the largest cluster among the particles identified as interface particles. The fluctuation of the local interface position is defined as $h(x_i, y_i) = z_i - \langle z\rangle$, with i the index of a particle on the surface and $\langle z\rangle$ the instantaneous average location of the interface. The irregularly distributed particle coordinates (x_i, y_i) are then mapped onto a regular grid in the xy plane with grid spacing $\Delta x = \Delta y = \sigma$ using Shepard interpolation [27]. Finally, the height fluctuation $h(\vec{q})$ is obtained from a Fourier transformation of the interpolated heights.

Figure 3 shows the q-dependent interfacial stiffness, as defined by the equation $\bar{\gamma}_1(q_x) q_x^2 + \bar{\gamma}_2(q_y) q_y^2 = k_B T/[L_x L_y \langle h^2(\vec{q})\rangle]$: for the (001) and (111) orientation $\bar{\gamma}(q) = \bar{\gamma}_1(q_x) = \bar{\gamma}_2(q_y)$ holds whereas for the (011) and (112) orientation there are two different coefficients $\bar{\gamma}_1(q_x)$ and $\bar{\gamma}_2(q_y)$ that can be determined from the latter equation by considering $q_y = 0$ or $q_x = 0$, respectively. The solid lines in Fig. 3 are fits of the data for $q < 1.5\sigma^{-1}$ with the

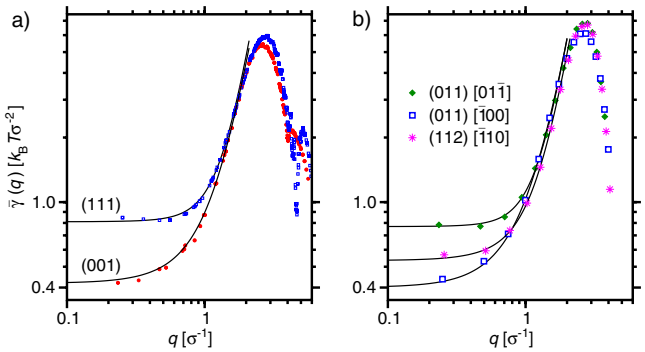

FIG. 3 (color online). q-dependent interfacial stiffness $\bar{\gamma}(q)$ for the (001) and (111) orientation (a) as well as the (011) and (112) orientation for the indicated directions (b). Note that for (112) only the [$\bar{1}$10] direction is shown because $\bar{\gamma}(q)$ for the [11$\bar{1}$] direction is very similar to that of the latter direction.

function $\bar{\gamma}(q) = \bar{\gamma} + aq^2 + bq^4$ yielding the values for the stiffness $\bar{\gamma}$ for $q \to 0$.

In Table I, the values of $\bar{\gamma}$, as obtained from our simulation, are given in comparison to previous simulation results and to DFT. A direct comparison is not possible since in DFT the *tensions* are calculated whereas in MC calculations the *stiffnesses* are measured. A comparison is only possible using a tension-stiffness conversion through a least-square fit to the tension anisotropy expansion (2) and the corresponding expression for the stiffnesses [through a combination of (2) and (1)], giving the average tension γ_0 and the parameters ϵ_i ($i = 1, 2, 3$). [Because the fit function (2) cannot reproduce the inner anisotropy for the (012) orientation (shown in the theory column of Table I) we have not taken into account the simulation data for the stiffnesses at the orientations (012) and (112) for the least-square fit. The different inner anisotropy therefore is not a shortcoming of DFT.] Here, an element of uncertainty is added by the truncation of the expansion since the single terms especially in the stiffness expansion are not small (note also the associated error bars in converted quantities).

As expected for a fcc-fluid interface, DFT shows the largest interfacial tension for the (001) interface orientation and the lowest one for the (111) orientation, giving the tension anisotropy $(\gamma(001) - \gamma(111))/2 = 0.025 k_B T/\sigma^2$. The average tension $\gamma_0 = 0.664 k_B T/\sigma^2$ is 7.4% higher than that from the simulation. This deviation most likely stems from the fact that in DFT (long-ranged) fluctuations in the interface are averaged out. A comparison between the stiffnesses shows deviations from up to 0.36 for the $(112)[\bar{1}10]$ direction to less than 1% for the $(012)[02\bar{1}]$ direction.

Previous simulations obtained the values $0.559(17) k_B T/\sigma^2$ [15] and $0.5610(12) k_B T/\sigma^2$ [17] for γ_0. These values are 10% smaller than our simulation results. An obvious discrepancy appears for the (111) interface orientation where we have not observed deviations from a fcc packing in contrast to [15]. Further differences to previous simulations are the use of a different geometry and of a rotational-invariant order parameter for the identification of crystalline particles.

We now compare our data to real-space experiments on dispersions of hard-sphere-like colloids. They often carry residual charges and are polydisperse. This renders a comparison with theoretical results on hard spheres difficult. Hitherto the interfacial tension was indirectly measured by interpreting the probability to find small (nonspherical) clusters in terms of classical nucleation theory [30] yielding data for a mean tension of about $\gamma_0 = 0.1 k_B T/\sigma^2$. Clearly, given the limitations of the hard-sphere model due to particle charging and the inherent assumption of small spherical crystalline nuclei, this is just a rough estimate of γ_0. An alternative experimental route is via the analysis of the capillary-wave spectrum similar to what we do in our MC simulations [31–33] providing direct access to the interfacial stiffnesses. In Ref. [32], the reported stiffness of $1.2 k_B T/\sigma^2$ for an interface between a randomly stacked hexagonal close packed (hcp) crystal and its melt is significantly higher compared to our results which might reflect the slight charge, the limited ensemble averaging, and an *ad hoc* value for the viscosity required for the analysis in this experiment. In Ref. [31], the reported stiffnesses were in the range of about $(0.7–1.3) k_B T/\sigma^2$. Interestingly, the stiffness for the (011) interface was found to be isotropic and the highest value for the stiffness was found for the (001) orientation, oppositely to what the authors expected and what we found for hard spheres. This might be due to a limited number of crystalline layers and the small gravitational length of $\sigma/7$ which limits the thickness of the liquid. Finally, Nguyen *et al.* [33] grew crystals of PNIPAM particles in a temperature gradient and analyzed the capillary waves along crystal-fluid interfaces after the removal of the temperature gradient. They measured averaged stiffnesses for several interface orientations in the range of $(0.19–1.13) k_B T/\sigma^2$ that show the best agreement with our results. Nevertheless, the latter experiment is also not accurate enough to validate theory and simulation on a quantitative level and thus more experimental explorations are required.

In conclusion, we have predicted accurate values for the anisotropic crystal-fluid surface tensions and stiffnesses of a hard-sphere system by using both fundamental measure density functional theory and Monte Carlo simulations. A small anisotropy in the tensions of about 10% was found which is, however, crucial for the transformation to stiffnesses which differ up to a factor of 4. These predictions can help to clarify apparent discrepancies found in real-space experiments of sterically stabilized colloidal suspensions [30–33]. Since the anisotropic tensions control changes of the interfacial shape, their precise quantitative determination help to understand crystal nucleation [34,35] and the transport of larger carriers through the interface. They may also serve as further input to phase-field-crystal calculations which explore solidification processes on larger length and time scales [36–38].

Future work should address soft interactions and attractions (as relevant, e.g., for colloid-polymer mixtures), in order to scan the full range from a fluid-crystal to a vapor-crystal interface. Further extensions can be done along similar ideas as used and proposed here for binary mixtures. Finally the recent extension of DFT towards dynamics for Brownian systems can be used to explore the time-dependent growth kinetics and relaxation towards equilibrium for the hard-sphere interface [39].

We thank K. Sandomirski and B. B. Laird for helpful discussions. This work was supported by the DFG via SPP 1296 and SFB TR6.

[1] J. Antonowicz, E. Jezierska, M. Kedzierski, A. R. Yavari, L. Greer, P. Panine, and M. Sztucki, Rev. Adv. Mater. Sci. **18**, 454 (2008) [http://www.ipme.ru/e-journals/RAMS/no_51808/antonowicz.html].
[2] N. V. Dziomkina and G. J. Vancso, Soft Matter **1**, 265 (2005).
[3] T. Gorishnyy, C. K. Ullal, M. Maldovan, G. Fytas, and E. L. Thomas, Phys. Rev. Lett. **94**, 115501 (2005).
[4] R. P. Sear, J. Phys. Condens. Matter **19**, 033101 (2007).
[5] D. P. Woodruff, *The Solid-Liquid Interface* (Cambridge University Press, Cambridge, England, 1980).
[6] W. A. Curtin, Phys. Rev. Lett. **59**, 1228 (1987).
[7] R. Ohnesorge, H. Löwen, and H. Wagner, Phys. Rev. E **50**, 4801 (1994).
[8] D. W. Marr and A. P. Gast, Phys. Rev. E **47**, 1212 (1993).
[9] W. A. Curtin, Phys. Rev. B **39**, 6775 (1989).
[10] H. Hansen-Goos and R. Roth, J. Phys. Condens. Matter **18**, 8413 (2006).
[11] M. Oettel, S. Görig, A. Härtel, H. Löwen, M. Radu, and T. Schilling, Phys. Rev. E **82**, 051404 (2010).
[12] T. Zykova-Timan, R. E. Rozas, J. Horbach, and K. Binder, J. Phys. Condens. Matter **21**, 464102 (2009).
[13] R. L. Davidchack and B. B. Laird, Phys. Rev. Lett. **85**, 4751 (2000).
[14] Y. Mu, A. Houk, and X. Song, J. Phys. Chem. B **109**, 6500 (2005).
[15] R. L. Davidchack, J. R. Morris, and B. B. Laird, J. Chem. Phys. **125**, 094710 (2006).
[16] M. Amini and B. B. Laird, Phys. Rev. Lett. **97**, 216102 (2006).
[17] R. L. Davidchack, J. Chem. Phys. **133**, 234701 (2010).
[18] R. L. Davidchack and B. B. Laird, J. Chem. Phys. **108**, 9452 (1998).
[19] T. Zykova-Timan, J. Horbach, and K. Binder, J. Chem. Phys. **133**, 014705 (2010).
[20] D. S. Fisher and J. D. Weeks, Phys. Rev. Lett. **50**, 1077 (1983).
[21] R. Roth, J. Phys. Condens. Matter **22**, 063102 (2010).
[22] Y. Rosenfeld, Phys. Rev. Lett. **63**, 980 (1989).
[23] P. Tarazona, Phys. Rev. Lett. **84**, 694 (2000).
[24] P. Pulay, Chem. Phys. Lett. **73**, 393 (1980).
[25] A. Kovalenko, S. Ten-no, and F. Hirata, J. Comput. Chem. **20**, 928 (1999).
[26] W. R. Fehlner and S. H. Vosko, Can. J. Phys. **54**, 2159 (1976).
[27] R. E. Rozas and J. Horbach, Europhys. Lett. **93**, 26006 (2011).
[28] P. J. Steinhardt, D. R. Nelson, and M. Ronchetti, Phys. Rev. B **28**, 784 (1983).
[29] P. R. ten Wolde, M. J. Ruiz-Montero, and D. Frenkel, Phys. Rev. Lett. **75**, 2714 (1995).
[30] U. Gasser, E. R. Weeks, A. Schofield, P. N. Pusey, and D. A. Weitz, Science **292**, 258 (2001).
[31] I. B. Ramsteiner, D. A. Weitz, and F. Spaepen, Phys. Rev. E **82**, 041603 (2010).
[32] J. Hernández-Guzmán and E. R. Weeks, Proc. Natl. Acad. Sci. U.S.A. **106**, 15198 (2009).
[33] V. D. Nguyen, Z. Hu, and P. Schall, Phys. Rev. E **84**, 011607 (2011).
[34] U. Gasser, J. Phys. Condens. Matter **21**, 203101 (2009).
[35] S. Auer and D. Frenkel, Adv. Polym. Sci. **173**, 149 (2005).
[36] K. R. Elder, M. Katakowski, M. Haataja, and M. Grant, Phys. Rev. Lett. **88**, 245701 (2002).
[37] H. Emmerich, Adv. Phys. **57**, 1 (2008).
[38] G. Tegze, L. Gránásy, G. I. Tóth, F. Podmaniczky, A. Jaatinen, T. Ala-Nissila, and T. Pusztai, Phys. Rev. Lett. **103**, 035702 (2009).
[39] S. van Teeffelen, C. N. Likos, and H. Löwen, Phys. Rev. Lett. **100**, 108302 (2008).